8-1975

Kinetics of the Thermal Decomposition of Pyridine

Tesfaye Biftu

KINETICS OF THE THERMAL DECOMPOSITION OF PYRIDINE

by

Tesfaye Biftu

A Thesis
Submitted to the
Faculty of The Graduate College
in partial fulfillment
of the
Degree of Master of Arts

Western Michigan University
Kalamazoo, Michigan
August 1975

ACKNOWLEDGEMENTS

The author wishes to express his appreciation to the members of his research committee, Dr. Donald Berndt and Dr. R. Steinhaus and especially to Dr. Thomas Houser for his generous assistance and guidance. The Ethiopian Spice Extraction Co., and especially its general manager Mr. Karl R. Sandelin, are also gratefully acknowledged for their support.

Tesfaye Biftu

TABLE OF CONTENTS

LIST OF FIGURES

INTRODUCTION

The primary objective of this work involved the study of the kinetics and mechanism of the thermal decomposition of pyridine in the gas phase using a stirred-flow reactor. Research was directed mainly at gathering kinetic and product distribution data which will help develop the mechanism of NO formation from fuel nitrogen during combustion. Pyridine was selected for this project because it is representative of the nitrogen containing components in fossil fuels, since the analysis of crude oil fractions show that most of the nitrogen containing compounds could be classified into pyridines, quinolines and carbazoles.[1]

Background

Even though comprehensive, homogeneous high temperature kinetic studies have not been reported, a few pyrolysis product studies were reported as early as 1962. Roth[2] was the first to study pyridine by passing this reactant through a red hot glass tube and noted HCN and bipyridine as the major products. Hurd and Simon[3] pyrolyzed pyridine and picoline at 825-850°C and reported benzene, benzonitrile, acetonitrile, acrylonitrile and quinoline as the volatile products.

A very limited rate study of the pyrolysis of pyridine and other nitrogen containing compounds was reported by Axworthy and Schuman.[4] The study was limited to the determination of % reaction and product distribution as a function of temperature in the interval of 950-

1100°C at a single contact time of 3/4 second and one entrance concentration. As such, the authors did not systematically determine the concentration dependence of the rate. They assumed a first-order rate dependence, and based on that, an activation energy of 70 Kcal/mole and a frequency factor of 2.5×10^{12} sec^{-1} were calculated.

Flow Reactor Theory

Flow systems are of two general types, those in which no stirring occurs in the reactor, i.e. plug-flow, and those in which sufficient stirring occurs so as to affect complete mixing within the reactor.[5]

If a mixture of gases is passed through a tubular reactor of a constant cross-sectional area and flow conditions characterized by the former case, the change in the number of moles of component i with time in a volume unit (dV) is given by

$$dn_i/dt = r_i dV - udc_i \qquad (1)$$

dV = cylindrical volume element

r_i = rate of chemical reaction

u = volume rate of flow of the reaction mixture

c_i = concentration of component i

At steady state, Eq. 1 becomes

$$r_i dV = udc_i$$

or

$$r_i = (u/dV)dc_i \qquad (2)$$

If, for constant flow systems, dV/u is replaced by dt, the resemblance between Eq. 2 and the usual equations for closed system kinetics becomes obvious.

$$r_i = dc_i/dt \tag{3}$$

If, instead of the tubular reactor, a stirred-flow reactor is used, the concentrations of the reactants and the products are considered uniform throughout the reactor and equal to the exit concentrations. Therefore, in Eq. 2 the volume element dV may be replaced by V (the total reactor volume), and dc_i may be replaced by $(c - c_o)$. Thus, Eq. 4 is obtained.

$$r = u(c - c_o)/V \tag{4}$$

c_o = initial concentration of component

Equation 4 applies to any component of the system. Again, if the flows are assumed constant, Eq. 4 can be rewritten

$$r = (c - c_o)/t \tag{5}$$

t = residence or contact time = V/u

Equation 5 enables an explicit determination of the rate of reaction. By changing the initial concentrations and/or flow rates, the form of the rate equation and the rate constants can be determined without requiring integration.

The above equations apply to any order reaction, simple or complex. For example, consider the simple first-order reaction

$$A \longrightarrow B$$

where

$$\text{rate} = -kc \tag{6}$$

Combining Eqs. 3 and 6 and integrating, the result for a tubular reactor is:

$$k = 1/t \ln (c_o/c) \quad (7)$$

c = concentration of A at time t

On the other hand, for a stirred-flow reactor, if Eqs. 5 and 6 are combined, the result is:

$$r = (c - c_o)/t = -kc$$

or

$$k = (c_o - c)/ct \quad (8)$$

Thus, integration is unnecessary to evaluate the rate constant in the case of the stirred reactor. For complex order reactions, functions of rate and concentration can be plotted relatively easily to determine the order.

Kinetic data obtained from stirred-flow reactors are called differential rate data since the differential rate is explicitly determined. If the extent of reaction in a plug-flow reactor is sufficiently low so that constant reactant concentrations can be assumed throughout the reactor, differential flow equations become applicable to that system also.

Another problem to be considered in the use of tubular reactor flow system is the effect of a volume change due to reaction on the rate of reaction. For example, consider the first order reaction.

$$A \rightarrow xB$$

x = any number but one

In this case, the volume rate of flow becomes

$$u = u_o[1 + (x - 1)(c_o - c)/c_o] \quad (9)$$

u_o = volume rate of flow without reaction

Using this value of u in Eq. 2, combining with Eq. 6, integrating and rearranging, Eq. 10 is obtained (for a first-order reaction only)

$$k = (u_o x/V)\ln(c_o/c)-(x - 1)(c_o - c)/c_o \qquad (10)$$

The equations for higher orders have been worked out,[6] however, their complexity discourages their use. In the case of the tubular reactor, the need for volume change correction can be eliminated either by maintaining low extents of reaction or by diluting the reactants with inert carrier gases. When using stirred reactors, this problem does not arise because the concentrations are uniform and explicitly determined; therefore, higher reactant concentrations can be used.

It can be concluded from the discussion on flow reactor theory that the stirred-reactor technique has two advantages:

1. Greater freedom in the selection of reaction conditions.
2. Kinetic data from complex order reactions can be more easily interpreted.

EXPERIMENTAL

Apparatus

A schematic representation of the flow system used in this study is shown in Figure 1. The system was constructed from Pyrex tubing except for the reactor which was made from Vycor, which allows reactor temperatures as high as 1200°C. Vycor, due to its very low coefficient of thermal expansion, insures a constant volume of the reactor despite the temperature variations. The reactor was joined to the flow system by 18/9 ball joint unions and this facilitated quick changes and cleaning.

Helium was used as the carrier gas and was purified by passing through activated charcoal. Carrier gas flow control was accomplished with a pressure regulator needle valve combination. The helium flow was monitored with a pre-calibrated capillary flow meter, F, containing dibutyl phthalate as the manometric fluid.

The carrier gas was heated in the preheater section which consisted of 10 mm by 20 cm Pyrex tubing wrapped with 22 B & S (16 ohms) gauge chromel resistance wire insulated by asbestos. The preheating helped to facilitate the vaporization of pyridine.

Pyridine was injected into the carrier gas stream at point S with a Sage model 237-2, motor driven, variable speed syringe drive. A 1.0 ml tuberculin syring was connected to a hypodermic needle, silver soldered into a metal ball joint which joined the needle and syringe assembly to the glass flow system. The rate of injection

LEGEND

C - Capillary
F - Flowmeter
P - Preheater
R - Reactor
CT - Cold Trap
⊖ - Ball Joint
⊗ - Stopcocks

S - Syringe
SC-3 - 3-way Stopcock
T(in) - Helium Purifier Trap
Z,Y - Valve through reactor and through by-pass respectively

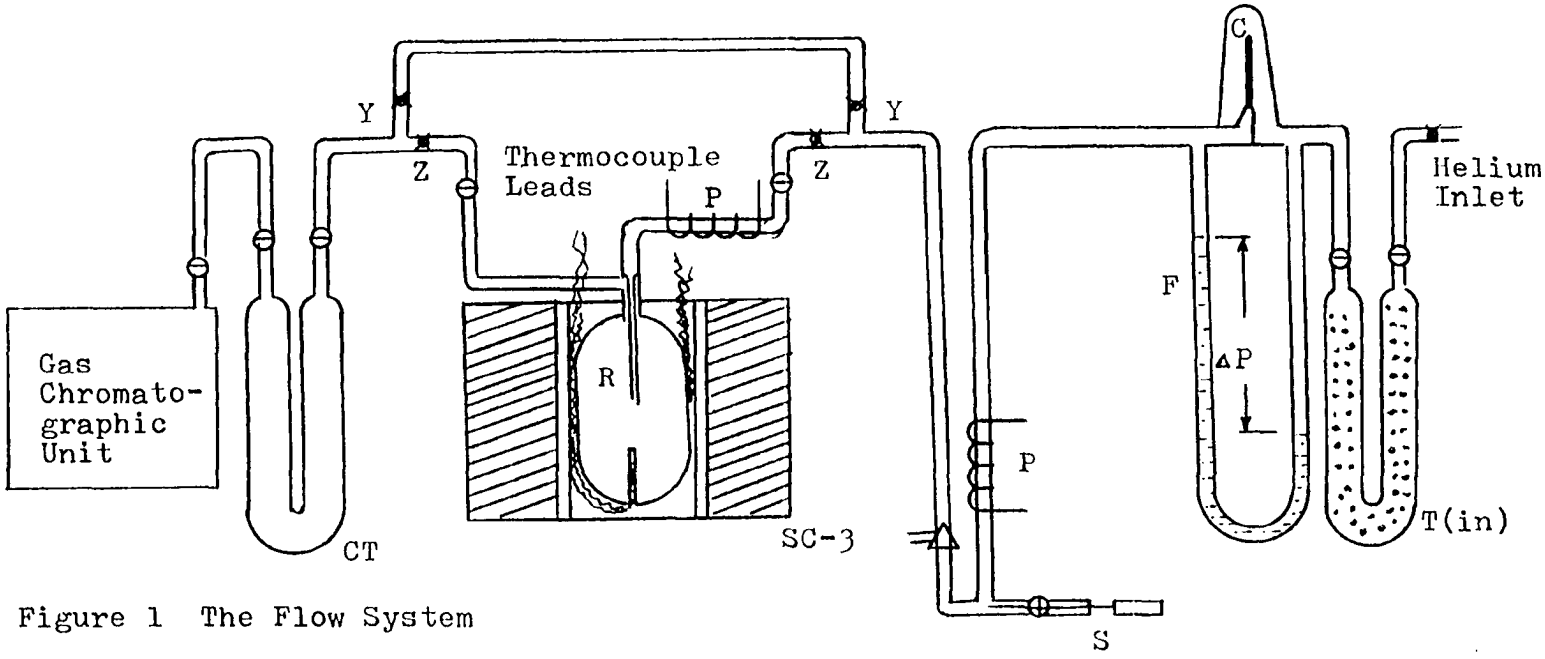

Figure 1 The Flow System

was dependent upon the syringe diameter, the gear configuration on the syringe drive, and the potentiometer setting which governed the speed of the drive motor. Injection was stopped and started manually.

After injection the gaseous mixture, having traveled about 3 feet from the point of injection and around five 90^{o} bends, was assumed homogeneous at the reactor entrance. It entered the reactor through a centered, 4 mm tube from which it jetted in all directions from pin holes near the reactor's center. Another 4 mm tube extended from the bottom to near the center of the reactor and served as a thermocouple well for temperature measurement. The reactor outlet was concentric with the inlet tube. There were three reactors, R, used in this study. The bulb portion of the largest reactor was 8 cm high and 4 cm in diameter with an effective volume of 64 ± 2 ml. The second reactor was 8 cm high and 3 cm in diameter with an effective volume of 39 ± 1 ml. The small reactor was 6 cm high and 1 cm in diameter with an effective volume of $6.5 \pm .5$ ml. The uncertainty in the reactor volume arose from the temperature gradient established along the inlet and outlet paths. In order that an explicit determination of differential rate data be attainable from this system, it is necessary that the reactor design affect complete mixing of the gas mixture, i.e. the concentrations of gaseous species in the exit stream were equal to those in the reactor. Previous experiments conducted by Sullivan and Houser[7] showed that the above assumption was valid for the type of reactor described.

Each of the reactors had a preheater coil (8 ohms of 22 B & S

gauge resistance wire) on the reactant entrance arm. This coil was connected in series with the gas pre-heater described earlier. The temperature was measured with a chromel-alumel thermocouple and a Honeywell Model 2732 portable potentiometer.

The reactor, shown schematically in Figure 2, was heated in an electric furnace formed by wrapping a 2 inch, diameter (I.D.), 1/8 inch thick cylindrical ceramic sleeve (Norton-Mullite) with two concentric windings (11 and 16 ohms of 16 B & S gauge resistance wire) extending its full length. Norton high temperature Alundum Cement served as insulating material near the windings. The outer winding was powered by a variac (1 KVA) which was connected directly to a 115 volt 60 cps line. The inner (controller) winding was powered by a variac (1 KVA) which was actuated (ON-OFF) by Honeywell, model MS 2, temperature controller. A chromel-alumel thermocouple placed between the reactor and the furnace wall, was used as a temperature sensor for the controller. A second thermocouple was placed in the thermocouple well of the reactor for temperature measurement. The insulating portion of the furnace consisted of an 8 inch breadth by 9 inch length and 9 inch high firebrick held together with steel pins, with a 2 inch hole at the center made for the electric furnace windings.

The gaseous mixture was allowed to flow through either the reactor or the by-pass. This was performed by the manipulation of the valves Z and Y in Figure 1. The mixture was then directed to a Beckman Gas Sampling Valve, which was attached to a gas chromatographic column. This column was made of up 5 feet of copper tubing, 1/4 inch in diameter.

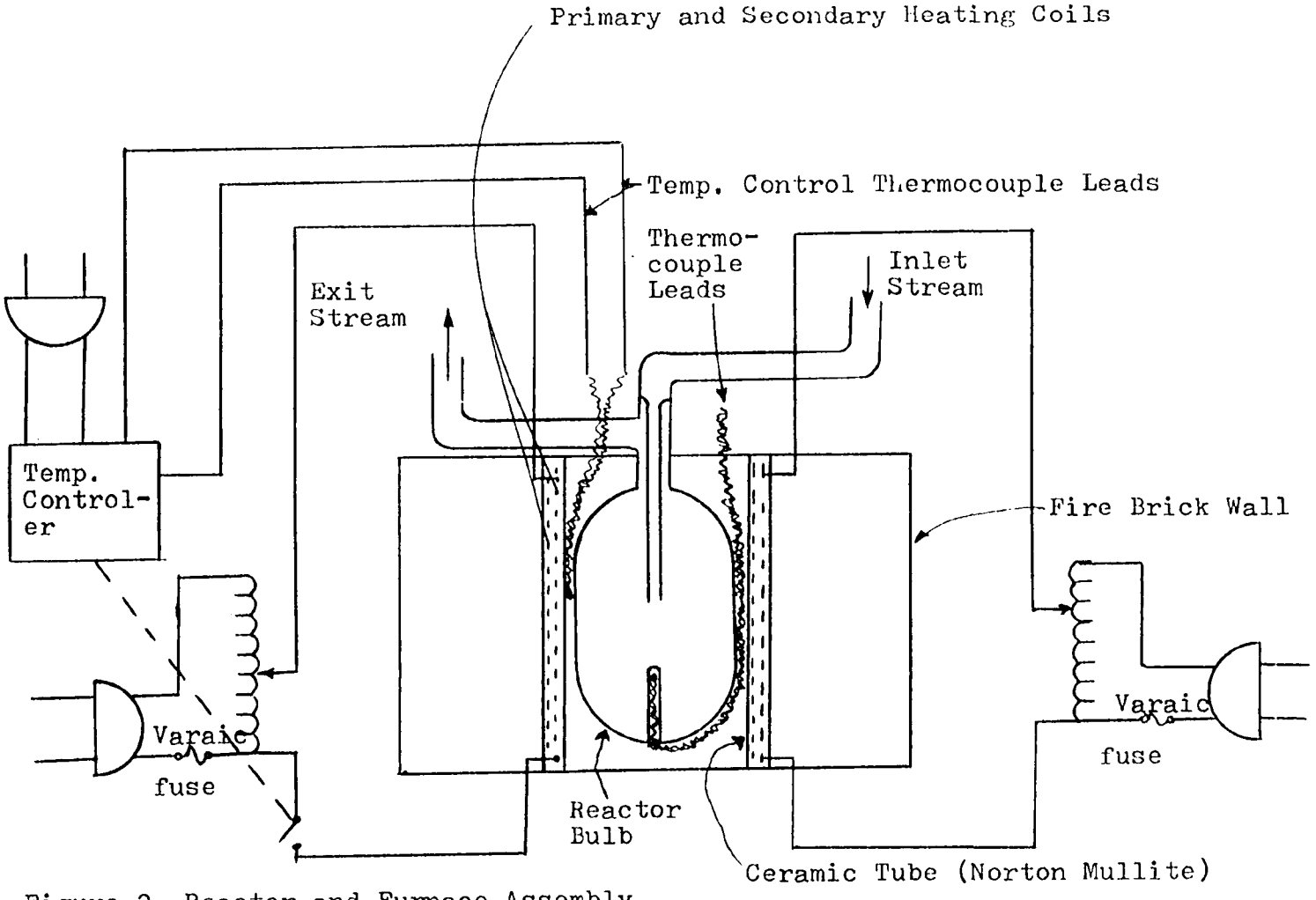

Figure 2 Reactor and Furnace Assembly

It was packed with chromosorb W acid washed DMCS (80/100 M) coated with 10% dinonyl phthalate. Helium was used as the carrier gas for the chromatograph. The helium flow was controlled by a needle valve and measured with a soap bubble flowmeter. The column was placed in a paraffin oil bath, the temperature of the oil was regulated as desired for efficient resolution of products. The range was 34-70°C. Two sample loops of 10 ml and 5 ml capacities were attached to the outlets of the sampling valve. In one position of the Beckman valve, a sample from the flow system could be injected from one loop into the gas chromatographic column, while a fresh sample was being received in the second loop, the valve can then be turned 90° and the respective positions of the loops reversed. The chromatographic detector used was a pair of matched thermistors mounted in a Gow Mac model 9766 cell. In order to minimize fluctuations due to temperature variation, the cell was fully protected with asbestos insulation. The power supply for the detector cell was a 12 V battery. The signal obtained was recorded on a Bristol model 64A-1PH760-51 strip chart recorder. The wiring diagram of the cell and recorder assembly is given in Figure 3.

Procedure

An experiment run in the medium reactor at 975°C, one second contact time and one mole percent pyridine in the carrier gas (975-1-1), is cited as an example for the experimental procedure used.

In this case, the desired reactor temperature, 975°C, was

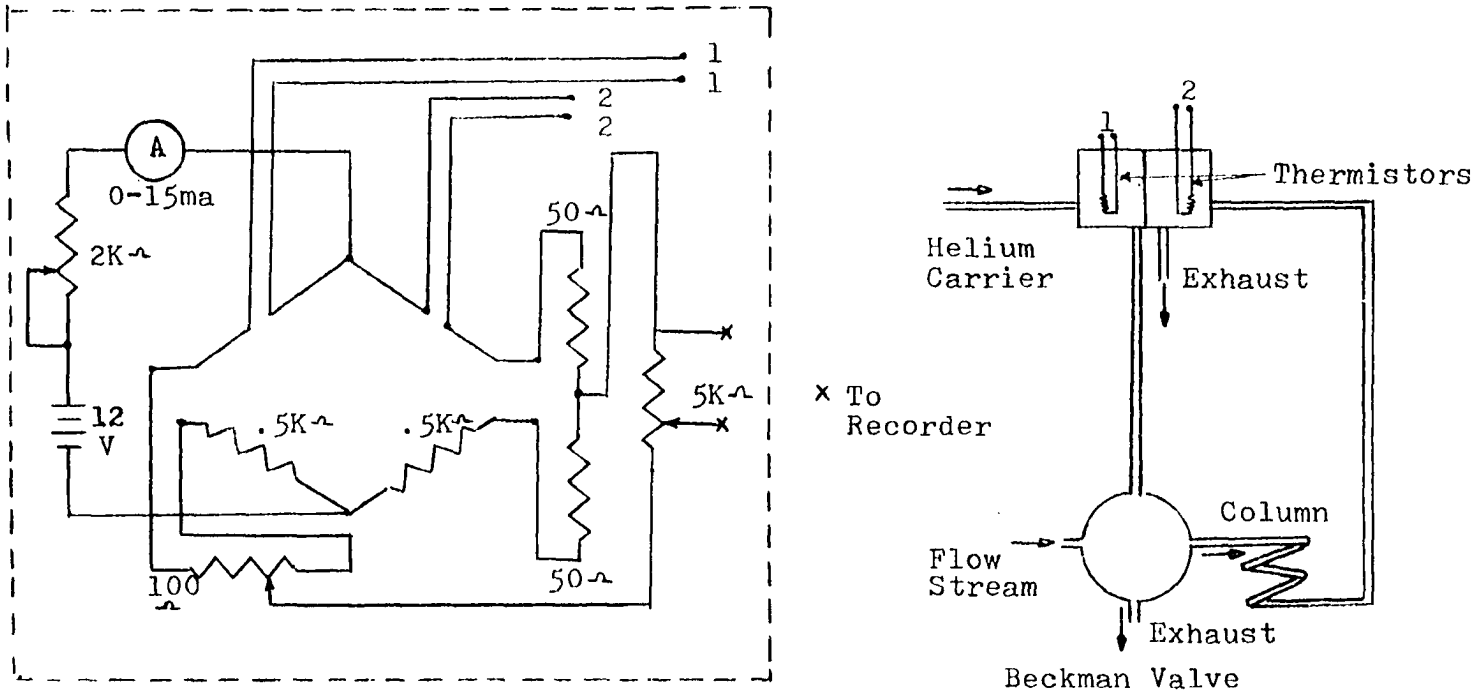

Figure 3 Wiring Diagram and Detector Assembly

ascertained by measuring the thermocouple output potential which corresponded to the number of degrees C above room temperature since the thermocouple's cold junction was at room temperature. Thus, a thermocouple output (corresponding to 975-25=950°C) of 39.34 mv[8] was necessary, and the temperature controller was adjusted until the desired output was attained. It was felt that the thermocouple well temperature was representative of the "true" reactor temperature and was used exclusively for subsequent calculations, temperature cycling never exceeded $\pm$ 1°C. This relatively high sensitivity resulted from having placed the controller sensor in the annular space between the furnace wall and the reactor which enhanced controller sensitivity. In addition, only 1/4 of the total power was obtained from the controller heater; thus, thermal inertial effects were minimized.

At each newly established temperature the reactor was conditioned and brought to steady-state. This was accomplished by injecting pyridine for at least 15 minutes under the conditions of reaction.

The carrier gas capillary flowmeter was calibrated with a "Precision" wet testmeter in terms of pressure drop (Δ p. cm of oil-dibutyl pthalate) versus flow rate (data in Appendix B). The pressure drop was found to be a linear function of flow rate. Under the conditions of run no. 975-1-1 the flow rate of helium was set at 12.1 cm (8.35 cc/sec at STP).

Syringe injection rates were calibrated by injecting n-dibutyl pthalate into weighed vials (data in Appendix B). Using a 1.0 ml

syringe a relationship between the drive potentiometer setting and rate of injection in μl of pyridine per second was obtained. In the case of run No. 975-1-1, a concentration of 1 mole % pyridine was desired; thus, the rate of injection of pyridine was set at 188 on the dial (.304 μl/sec.).

Having established the conditions to give the desired reactant concentration and contact time, the following procedure was applied: Prior to connecting the needle to the flow apparatus, helium was allowed to flow through the entire system for about 5 minutes; this insured the removal of any residual volatile material and also flushed out oxygen. After filling the syringe and affecting the removal of all air in the syringe and the hypodermic needle, the injection system was assembled and inserted into the flow system. With the helium flow properly adjusted, the three-way stopcock, SC-3, was set so as to vent the system to the room. The syringe drive motor was actuated until it could be ascertained that the syringe plunger had been displaced. This assured the removal of mechanical slack in the drive system. The gas chromatographic carrier gas valve was opened and the flow rate adjusted to 100 ml/min. After 5 minutes of helium flow the gas chromatographic cell unit was turned on. This assured the removal of oxygen from the cell.

The by-pass stopcocks were opened and the stopcock, SC-3 was changed so as to direct the helium flow through the by-pass, then, the syringe drive was actuated. The tip of the hypodermic needle,

from which pyridine was vaporizing, was carefully observed to insure that no liquid reactant was being injected into the gas stream; such an occurence would lead to poorly defined concentrations. Adjustments of the power to the preheater section would eliminate such a problem. After 10 minutes of flushing, the recorder was actuated and adjusted to the zero line. The chart speed was kept at 1 inch per minute. Having the temperature, and the helium and pyridine flow rates under control, the sample was injected into the gas chromatographic column kept at 69°C. This was done by turning the knob on the Beckman sampling valve to position A. One minute after pyridine was eluted, another sample from the second loop was injected by turning the sampler valve back to position B. The process was repeated until a reproducible peak height was obtained. In the present case the sensitivity was set at 650 and the peak height recorded for the sample injected from the 10 cc sample loop was 14.2 cm. Having established the peak height that corresponded to the unreacted pyridine, the valves leading to the reactor were opened and those to the bypass closed. The reactor was flushed for 15 minutes prior to the injection of a sample into the column. In this case, the recorded peak height was 9.6 cm. From the peak heights before and after decomposition, the extent of reaction was determined to be 32.4%

The reactant concentrations studied were kept below 2 mole per cent, as condensation of pyridine took place in the flow lines if concentrations exceeded this quantity. Hence, the volume changes accompanying the reactions were fairly low and as such there were no corrections made for these.

Materials

A reagent grade pyridine was obtained from Matheson, Coleman, and Bell. Each 300 ml portion was treated with 25 g of KOH (U.S.P.) and distilled over $CaCl_2$. This eliminated the trace amount of water absorbed.

Analytical Techniques

The volatile products and reactant were analyzed by the gas chromatographic unit which was linked to the flow system. The extent of reaction and the final concentration of reactant were determined directly from the ratio of the initial and final peak heights as measured on the strip chart recorder.

Height of HCN peaks were also measured and standardized by dividing them by the peak height of one mole percent pyridine at the same chromatographic conditions. The concentration of HCN was also measured by the Liebig[9] method. HCN was trapped by passing the voltaile products through 2.5% solution of KOH in distilled water. Silver nitrate does not react with any of the volatile products except HCN. It reacts with CN^- in alkaline solution as follows:

$$Ag^+ + 2CN^- = Ag(CN)^-_2$$

Hence, any precipitate formed dissolves as long as CN^- is in excess. However, any excess Ag^+ will result in a turbid solution due to the formation of AgCN and this turbidity was used as an end point indicator. One ml of N/10 $AgNO_3$ was equivalent to 2×10^{-4} moles of HCN.

Having the results from the titration and the standardized peak heights, a calibration curve was constructed (data in Appendix B). The relation was as follows:

HCN concentration (mmoles/l) =

(.00117)(standardized peak height)

The composition of the condensable volatile product was determined after trapping the reaction products with liquid nitrogen, by gas chromatographic-mass spectrometric analysis with an LKB GC-MS (type 900) instrument through the courtesy of the Upjohn Company. Also, a high resolution mass spectrum was obtained with an Atlas mass spectrometer through the courtesy of the Upjohn Company for the total volatile mixture received in a gas syringe from the exit line of the reactor. This mixture was also analyzed by gas chromatographic-mass spectrometric analysis on Dupont Model 21-490 B instrument. A mass spectrum of the solid product from the reaction carried out at 950°C was obtained on the latter instrument using a solid probe. An elemental analysis of the solid products from 950 and 1000°C was made by Galbraith Labs. Inc. of Knoxville, Tennessee.

Sample Calculations

The results from run No. 51 with the medium reactor is cited and the reaction rate was calculated as follows:

For this reactor the conditions were:

initial concentration of pyridine in the gas stream = 1.00 mole percent

contact time = 1.00 sec.

Flow rate at 975°C and 745 mm Hg =

volume of reactor/contact time =

39.2 cc/1.00 sec. = 39.2 cc/sec.

Flow rate at STP =

(273)(39.2)(745)/(273 + 975)(760) = 8.43 cc/sec.

After correction for the 1% pyridine, the flow rate of helium = 8.43 (1 - .01) = 8.35 cc/sec: thus Δp from the calibration data in Appendix B = 12.1 cm. The rate of injection of pyridine = molecular weight of pyridine x mole fraction of pyridine x total gas flow rate/ density of pyridine x 22.4 = (79.1 g/mole x .0100 x 8.43 cc/sec)/ 22,400 cc/mole x .978 g/cc) = $.304 \times 10^{-3}$ cc/sec = .304 μl/sec: thus the potentiometer drive setting = 620 x rate of injection, = 620 x .304 = 188.

Thus, the initial concentration = c_o = (.01) P/RT = (.01) (745)/(760)x(.0821)x(273 + 975) = $.0957 \times 10^{-3}$ moles/l = .0957 mmoles/l.

The extent of reaction = F =

1 - (peak height of pyridine through the reactor/peak height through the by-pass) = 1 - (27.1/40.0) = .322.

Change in concentration = X = $c_o F$ = .0957 x .322 = .0308 mmoles/l.

Hence,

rate = r = X/t = .0308/1.00 = 0.0308 mmoles/l sec.

r/c = $r/(c_o - X)$ = $F/(1 - F)t$ = 0.0308/(0.0957 - 0.0308) = .475

RESULTS AND DISCUSSION

Reaction Products

Volatile Products. The relative amounts of volatile products were very low at low operating temperatures and increased as the temperature increased. At 900°C the highest extent of reaction achieved was 27.8% at 4 sec contact time and 1 mole % pyridine in the gas stream; no volatile product was detected at this condition. At 925°C the highest extent of reaction was 28.4% and again no volatile product was detected. At 950°C and extents of reaction higher than 11% two product peaks were obtained; at 975 and 1000°C in all experiments, three additional peaks showed up.

The gas chromatographic column was normally run at 70°C. This shortened the retention time of pyridine (140 sec) and permitted faster analysis of pyridine consumption. However, at this temperature resolution between some of the volatile products was not obtained. To get a better separation, the column temperature was set at 42°C and 34°C. A good separation between the volatile products was obtained at 34°C. The retention times of all the exit gases along with the compounds to which they are believed to correspond are shown in Table I.

Volatile reaction products at 975°C and 65% extent of reaction trapped by liquid nitrogen gave six peaks when passed through the chromatograph of the mass spectrometer. The first three peaks were very close and a mass spectrum was obtained for the mixture. Mass spectra were obtained for the last three peaks also. The relative abundance of

the most predominant ions along with the compounds to which they correspond are shown in Table II.

TABLE I

Gas Chromatographic Data

No.	Retention Time, Sec. Products	Knowns	(34°C Column Temp.) Compound
1	18	16	Acetylene and/or methane or ethylene
2	-	35	1-Butene-3-yne[a]
3	49	-	HCN[b]
4	106	-	Diacetylene[c]
5	132	130	Propenenitrile
5	232	230	Benzene
6	760	760	Pyridine

a) Mass spectrometer suggested the presence of this compound. However, no appreciable peak was obtained on G.C.

b) Identified by odor initially, and later mass spectrometrically.

c) Suggested by mass spectrometer data, a known was not available to check its retention time.

To more quantitatively illustrate the shift to larger amounts of volatile products at higher temperatures, it was found that at 950°C and 24% reaction, the ratio of HCN peak height to that of 1% pyridine was .05 (HCN peak height was 5% of the peak height of 1% pyridine in the gas stream). At 1000°C and 22% reaction, the HCN peak height was

TABLE I

Mass Spectral Data

No.	Product[a]			Compound	Knowns[10]					
1.	27/100	26/93	50/93	A. Acetylene	26/100	25/19	24/5	13/3	27/2	12/1
	28/64	52/60	49/38	B. Hydrogen Cyanide	27/100	26/17	12/4	13/2	14/2	28/2
	51/37	48/9	37/5	C. Diacetylene	50/100	49/36	25/10	48/8	37/5	51/4
	12/5	13/4	25/3	D. 1-Buten-3-yne	52/100	51/50	50/42	49/13	26/11	37/5
				E. Ethylene	28/100	27/63	26/53	25/8	29/12	14/2
2.	52/100	26/100	53/100		53/100	26/100	52/75	51/32	27/18	25/18
	51/41	27/21	50/10	Propenenitrile						
	28/10	25/8	38/7							
	54/7	37/3	24/2							
3.	78/100	77/94	52/77		78/100	52/18	51/17	77/15	50/14	39/11
	51/65	50/53	79/48	Benzene						
	76/30	74/26	39/24							
	75/10	38/10	73/8							
4.	79/100	52/100	51/92		79/100	52/71	51/36	50/26	78/12	39/12
	50/82	78/55	80/42	Pyridine	79/100	52/100	51/100	50/100	53/94	78/94[b]
	39/29	53/28	26/16							
	49/13	28/10	75/9							

[a]Mass spectra of products are from a condensed sample. Numbers are mass no. of ion/relative intensity of ion.

[b]Mass spectrum of pure pyridine at the same conditions the spectra of the other volatile products were obtained.

14.3% of a 1% pyridine peak height. At 975°C and 50% reaction, HCN had a relative peak height of 15.9%. At the same condition, (50% reaction) the amounts of benzene and propenenitrile were about equal and they had peak heights of 14% of the respective HCN peak.

It should be noted that acetonitrile reported as a product in earlier investigations[4], had a retention time of 109 sec and this matched with the product peak at 106 sec. However, none of the mass spectra gave a significant signal at an m/e of 41, including the mass spectra of the total gas sample. According to previous studies made by Houser and Asmus[11] the extent of reaction of the thermal decomposition of acetonitrile at a temperature and residence time of 960°C and 4 sec respectively was about 40%. Hence, the conditions of the experiment did not favor the existence of this product on a large scale. Thus it is concluded that acetonitrile is not a significant product.

Mass 27 peak was further analyzed using a high resolution mass spectrometer and the exact mass was found to be 27.0110 which agreed with the mass of HCN which is 27.0109[12]. Mass 28 also gave a small peak with an exact mass of 28.0314, indicating the presence of a small amount of ethylene. The total gas sample showed a split of m/e 16, indicating the presence of methane.

Solid product. A brown, non-volatile, polymeric material formed by the reaction coated the walls of the reactor outlet. This residue was soluble in acetone and dimethylsulfoxide. According to quantitative elemental analysis, the solid product formed at 950°C, 1.00 sec residence time and 1.00% initial pyridine concentration had the composition

78.6% C., 4.3% H and 16.2% N. At 1000°C, 1.00 sec contact time and 1.00% initial pyridine concentration, 85.0% C, 3.8% H and 10.4% N were found. As the composition of the residue depends on the amount of non N containing volatile products, no conclusion could be reached as to what the theoretical N content in the residue should be. The decrease in the nitrogen content of the residue at the higher experimental conditions was consistent with the results from the previous workers[4] as most of the nitrogen was in the residue at low temperature, while most of it was converted into the volatile products, specifically HCN, as the temperature increased. It was also found that once the residue was formed, further heating did not produce HCN. This shows that the HCN formed in the high-temperature pyrolysis experiment forms directly in the initial pyrolysis reaction.

The infrared spectrum of the residue showed major absorptions at 2200 cm^{-1} and 1625 cm^{-1} which corresponded to C ≡ N and C = C stretches respectively. The NMR spectrum showed signals in the range δ = 7.6 - 8.8. This pattern is charcteristic of complex aromatic compounds. The mass spectrum had grouped signals. Taking the most intense mass number from each group, the order in terms of decreasing relative abundance was (including the compounds which may have given rise to these groups of ions) 154 (biphenyl, bipyridine), 128 (napthalene, quinolines), 179 (acridine, benzoquinoline), 104 (styrene), 117 (indole), 203 (pyrene with one nitrogen in a ring), and 167 (carbazole). The following groups of ions also were observed and could have come from several of the above compounds 51, 79 and 101. This is not intended to be a comprehensive listing of all species, but represents groups which are probably pre-

sent in the solid. A full characterization of the solid would be a complete research project in itself and of questionable value for the overall objectives of this project.

It should be noted that the concentrations of HCN produced during the reaction at 1000°C, as determined from chromatographic measurements, were too large, i.e., the (HCN) was larger than the change in (C_5H_5N). Thus, other species may be contributing to this peak during kinetic experiments, or the uncertainty in the measurements was larger than expected. It appears that a more reliable method of (HCN) measurement will have to be developed to determine its rate of formation.

Kinetic Results

The results produced by flow experiments are illustrated in Figures 4 through 8 and the data are shown in tabular form in Appendix A. At low operating temperatures, the fraction of pyridine decomposed, F, was independent of initial pyridine concentration. However, at higher temperatures the value of F increased as the initial concentration increased.

It was found that the rate expression which best fit the data was of the form:

$$r = X/t = k_1(c_o - X) + k_2(c_o - X)(X) \qquad (11)$$

where $X = c_oF$ = change in reactant concentration, mmoles/l

k_1 and k_2 are first and acceleration rate constants

F is the fraction reacted

r is rate, mmoles/l sec.

The rate constants, k_1 and k_2, for the medium reactor at the four higher temperatures were determined from the least squares intercepts and slopes of plots of r/c versus X, Figures 5 and 6; at 875 and 900°C the rate followed a first order equation and k_1 was determined from slopes of the plots of r versus c (Figure 4). These results are presented in Table III. The correlation coefficient was calculated at each temperature for the functions plotted and the values were .997, .949. .827, .680, .862, and .905 at 875, 900, 925, 950, 975 and 1000°C respectively. F-tests also showed that the calculated rate constants and functions represented the data with a probability of at least .99 (except at 950 the probability was about .95). Analysis of uncertainties is given in Appendix C.

TABLE III

Kinetics Results (Medium Reactor)

T °K	$1/T \times 10^3$	k_1[a] sec^{-1}	-log k_1	k_2[a] l $mmole^{-1}sec^{-1}$	logk_2
1148	.871	.090 ± .002	1.046	-	-
1173	.854	.158 ± .015	0.801	-	-
1198	.836	.249 ± .020	0.604	2.87 ± .69	.458
1223	.818	.367 ± .033	0.435	3.74 ± .79	.573
1248	.801	.404 ± .078	0.394	11.47 ± 1.51	1.059
1273	.786	.986 ± .25	0.061	36.71 ± 3.09	1.565

[a]The ± values are one standard deviation.

Analysis of Arrhenius plots (Fig. 7 & 8) of the first-order and acceleration rate constants lead to the following expressions for the rate constants.

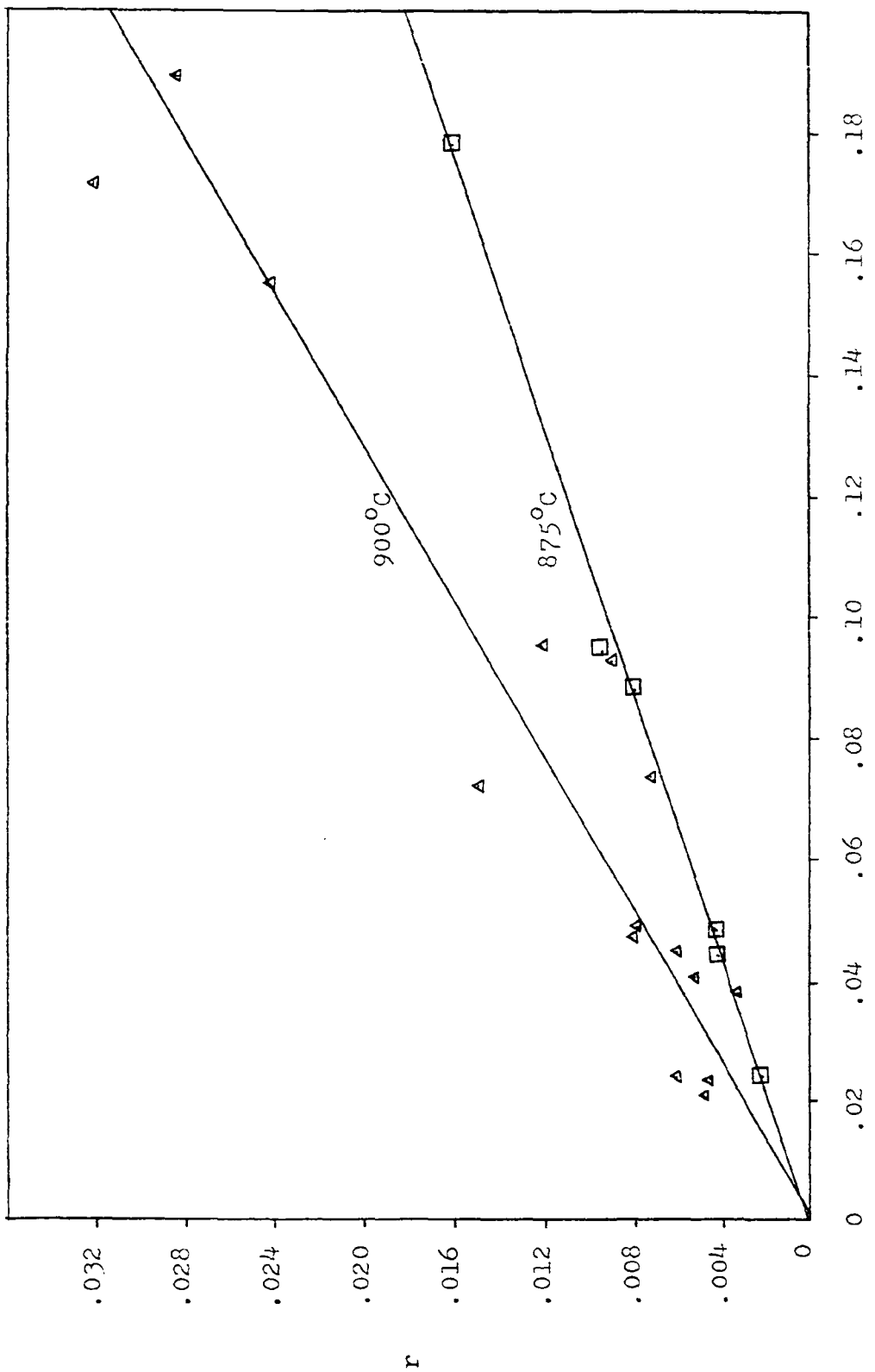

Figure 4 Plot of Rate Data at 875 and 900°C.

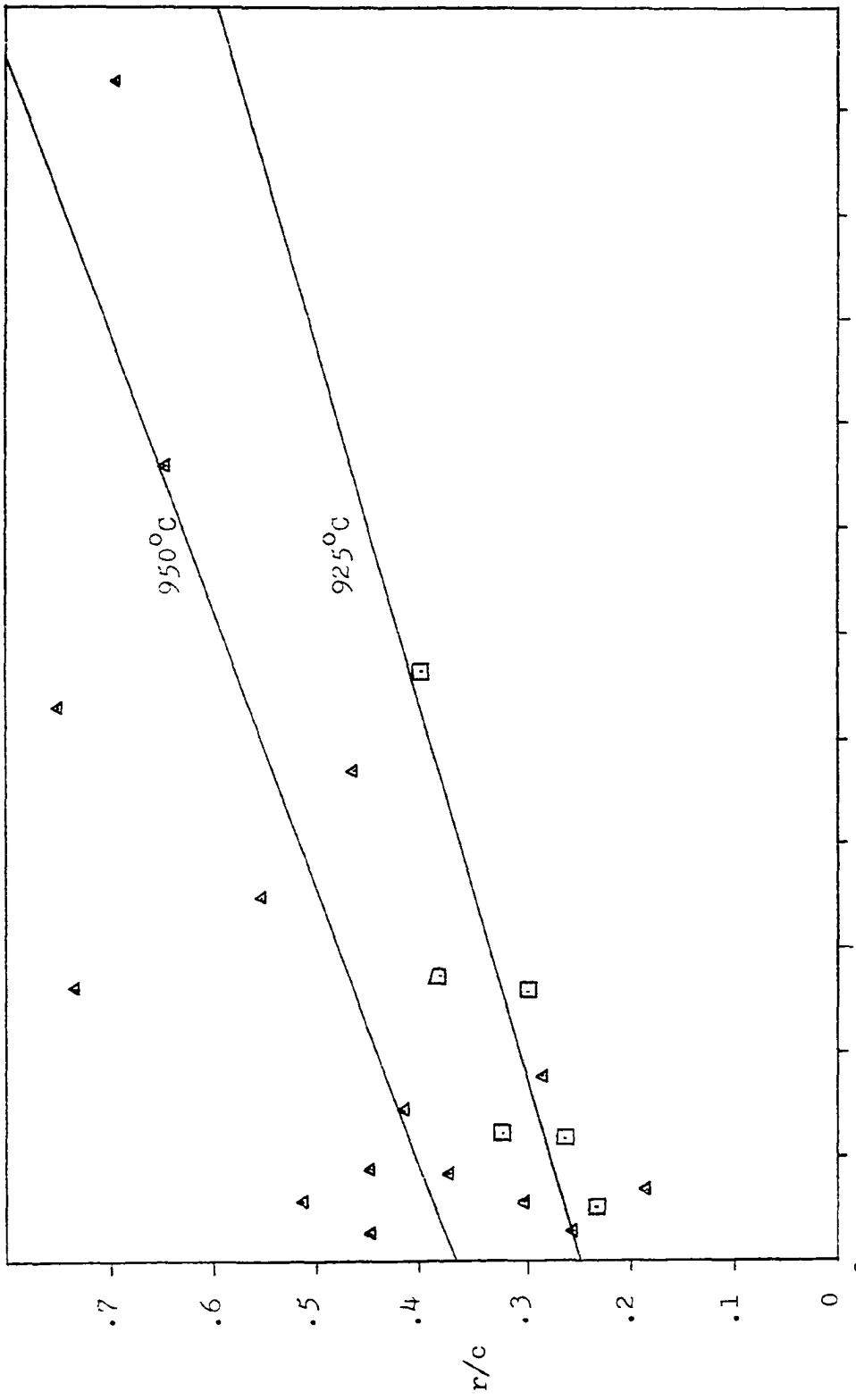

Figure 5 Plot of Rate Data at 925 and 950°C

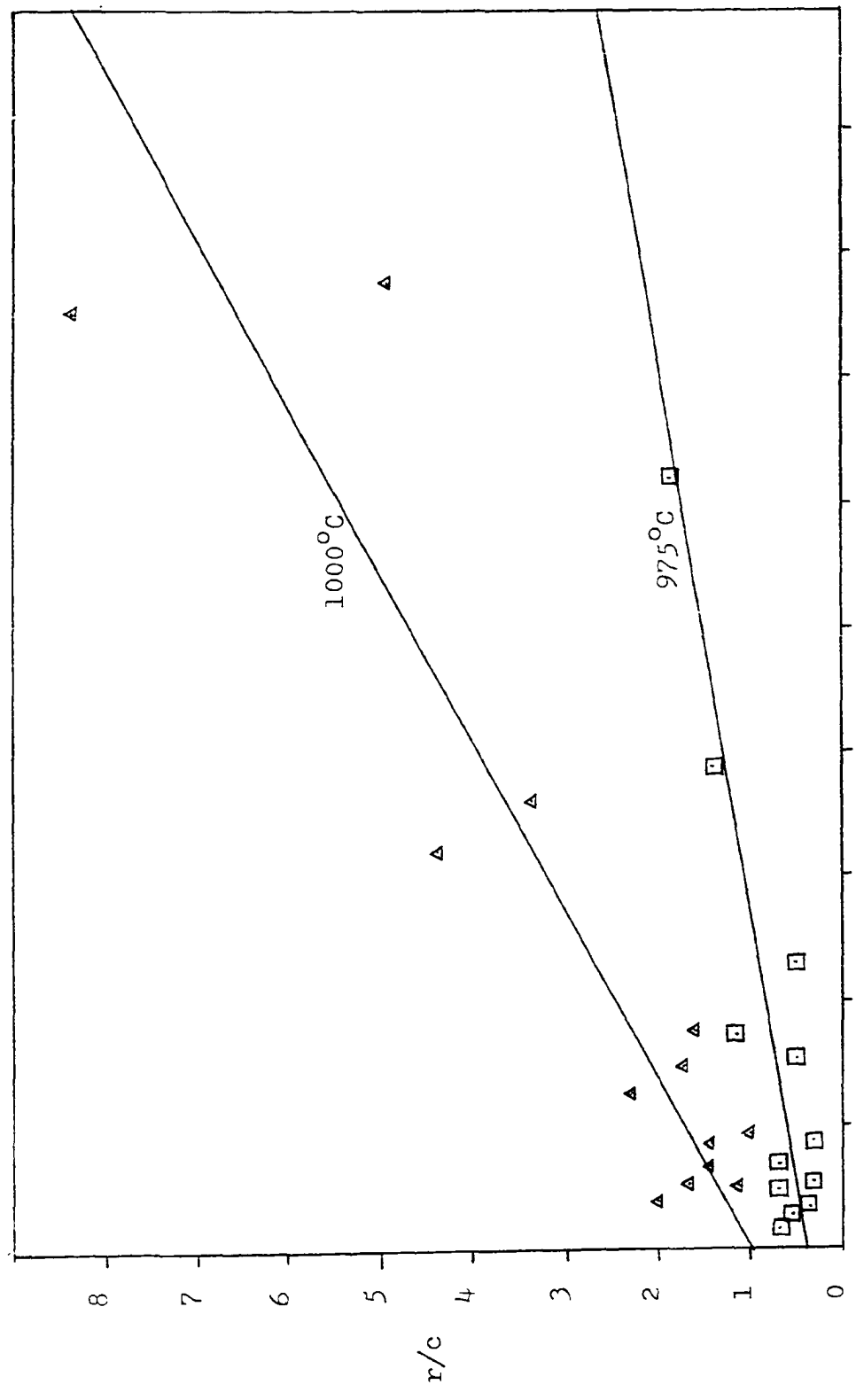

Figure 6 Plot of Rate Data at 975 and 1000°C.

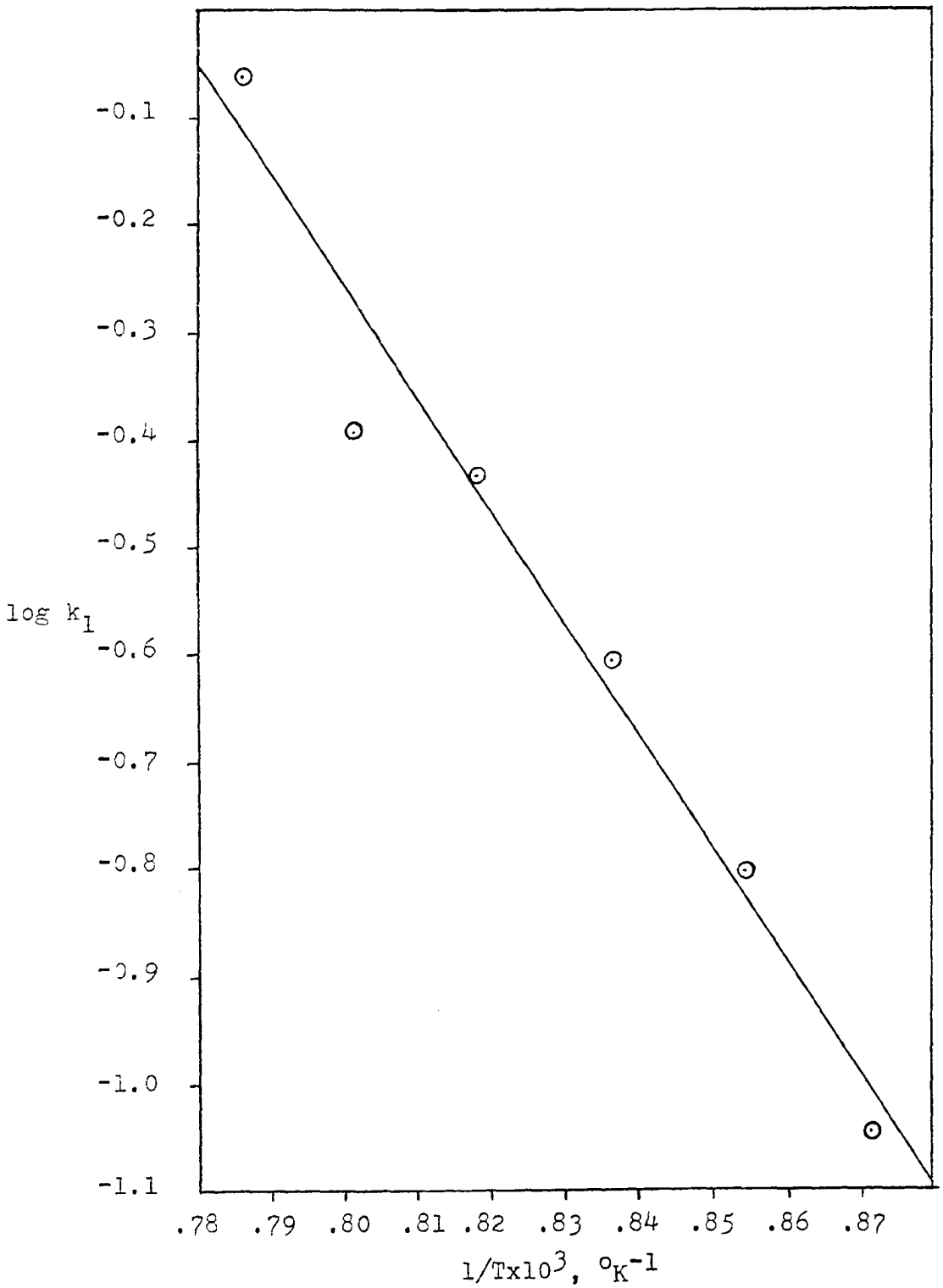

Figure 7 Arrhenius Plot (first order rate constants)

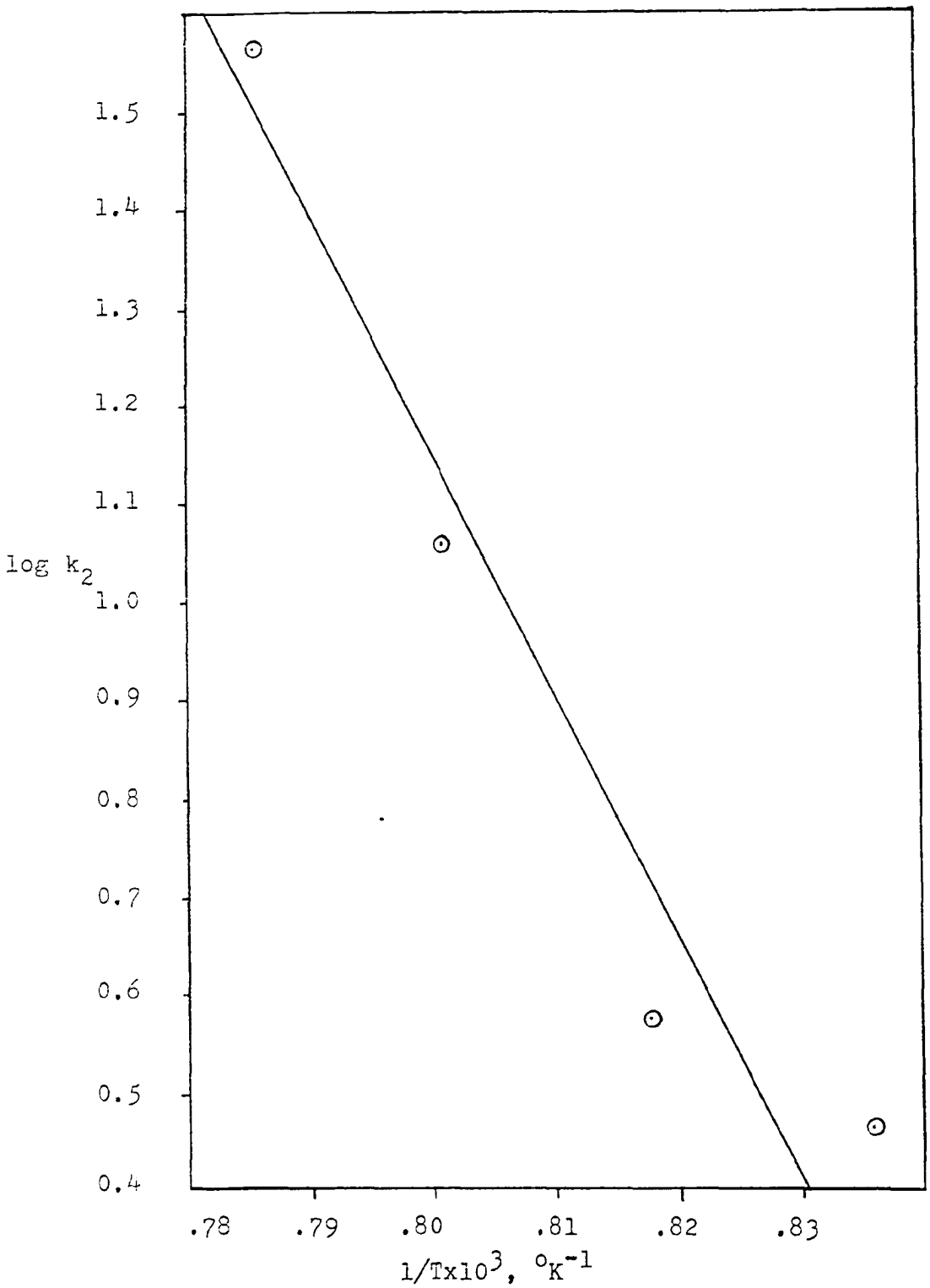

Figure 8 Arrhenius Plot (acceleration rate constants).

$$k_1 = 10^{8.2 \pm .5} \exp-(48{,}200 \pm 2{,}800)/RT(sec^{-1})$$

$$k_2 = 10^{20.8 \pm 1.9} \exp-(112{,}000 \pm 11{,}000)/RT(l/mmole\ sec)$$

In finding the Arrhenius constants the rate constants, k_1 and k_2, were weighted according to the number of data points.

Twenty five rate equations, where orders of 1/2, 1, 3/2, 2 with respect to each of the reactant and fraction product were considered. However, all trials ended up with uncertainties substantially higher than those obtained with equation 11.

Surface Effects on the Rate

The medium reactor has a volume of 39.2 cc and surface area of 107 cm^2, thus, the effective surface to volume ratio was 2.73. For the small reactor the volume was 6.5 cc while the surface was 58.3 cm^2 and its effective surface to volume ratio was 8.97. As such, the small reactor had an effective surface to volume ratio which was about three times as large as the medium one. The rate constants k_1 and k_2 for the small reactor at 975 and 1000°C are given in Table IV (data in Appendix A).

TABLE IV

Kinetics Results (Small Reactor)

T °K	k_1 $sec.^{-1}$	k_2 1 $mmole^{-1}sec.^{-1}$
1248	0.116	7.41
1273	0.358	13.47

The surface effect is clearly demonstrated by comparing the values of k_1 and k_2 from Table IV with their corresponding values from Table III. Increasing the surface by three fold gave k_1 and k_2 values which were only about 1/3 the original value for both constants. This decrease in rate as the surface increased shows that the reaction was complex in character, that recombination of atoms or free radicals was occuring at the surface and these radicals were involved in both terms of the rate equation[13]. A third reactor tested had an effective surface to volume ratio of 1.99 and a similar phenomena as the one discussed above took place (data in Appendix A). The formation of HCN also followed the same path and as such, its formation was enhanced as surface to volume ratio decreased. For the reactor with the largest surface area the HCN and other volatile products were very low possibly due to recombinations taking place prior to fragmentation into the volatile products.

Acceleration Effect of CN

From the equation that best describes the kinetic data, a fraction of the product was found to be responsible for the acceleration effect. The possible acceleration effect of CN was tested by introducing a 2% $(CN)_2$ with the carrier gas. An increase in percent reaction by a factor greater than two was observed due to CN (data is given in Appendix A).

The equation $r/c = k_1 + k_2\,(HCN)$, which was similar to eq. 11 where one assumes HCN is the sole product having an accelerating effect

on the decomposition of pyridine, was also considered. However, it was not possible to obtain k_1 values as they turned out to be negative. This suggested that the acceleration was due to other products or intermediates, not only HCN.

Reaction Mechanism

An acceptable mechanism for the pyrolysis of pyridine should account for:

1. the origin of all observed products
2. the observed rate law for the reaction, i.e. $-d(c)/dt = k_1(c) + k_2\ (c)(X)$
3. the low activation energy and frequency factor associated with the first-order rate constant
4. the high activation energy associated with the acceleration term rate constant
5. the rate decrease as the surface to volume ratio increased.

The pyrolysis of pyridine occurs by a complex mechanism which does not permit the elucidation of a detailed mechanism from the data of the rate of disappearance of pyridine alone. This requires a further study of the rates of formation of the volatile and non volatile products. A generalized chain mechanism that meets the requirements for the first-order term based on available data is as follows:

Initiation:

$$P \longrightarrow R + H \qquad 1$$

Propagation:	$P + H \longrightarrow R + H_2$	2
	$2R \longrightarrow$ Product + 2H	3
Termination:		
	2R (surface)$\rightarrow$ Product	4

The initiation step is assumed to be a C-H break rather than a C-C or C-N break since the later would involve a higher activation energy. The solid residue is believed to form by the surface recombination of radicals giving a polymeric product or other non volatile products such as bipyridine, benzoquinoline, etc.

The steady state treatment of this mechanism with the assumption that rate 1 $\ll$ rate 2 or rate 3 gave the following expression:

$$\text{rate} = (k_3k_1/k_4)P$$

This leads to the following expression for the theoretical activation energy:

$$Ea = E_3 + E_1 - E_4$$

The C-H bond energy is 95-100[14] Kcal/mole. Assuming E_1, E_3, and E_4 to be 95-100, 0-10, 0-10 Kcal/mole respectively, a theoretical activation energy of 95-100 Kcal/mole is obtained. This value is inconsistent with the observed first-order activation energy of 50 Kcal/mole.

Other conventional chain mechanisms (e.g. Rice-Herzfeld type) were rejected because they require fragmentation of radicals, thus, should lead to volatile products rather than solid products.

Another possibility is a polymer chain mechanism which is suggested as follows:

Initiation:

$$P \longrightarrow R_1 + H \qquad 1$$

Propagation:

$$P + R_1 \longrightarrow R_2 + H_2 \qquad 5_a$$

$$P + R_2 \longrightarrow R_3 + H_2 \qquad 5_b$$

Termination:

$$P + R_i \longrightarrow \text{Product (surface)} \qquad 6$$

This leads to the following rate expression:

$$\text{rate} = (k_5 k_1 / k_6)\ P$$

where the rate constants for the propagation reaction were all assumed to be the same. In this case the value of the theoretical activation energy is given by:

$$E_a = E_5 + E_1 - E_6$$

Even though, E_1 is 95-100 Kcal/mole the value of E_a is dependent on E_5 and E_6. A relatively small E_5 value combined with a high E_6 could give an E_a which is relatively consistent with the observed first order activation energy.

To satisfy the requirements imposed by the second term in the rate equation, an auto catalytic reaction is proposed; the mechanistic detail for such a reaction path is highly speculative. The high activation energy associated with this reaction is probably due to more fragmentation of the ring and indicates that the reaction is not a chain process, but could be a series reactions as follows:

$$\text{Pyridine} \longrightarrow \text{radicals} \longrightarrow \text{volatile products}$$

$$\text{Pyridine + radicals (product)} \longrightarrow \text{products}$$

The radicals formed in this sequence are different than those formed in the lower temperature process as indicated by the volatile product formation. Some possible examples are as follows:

$$P \longrightarrow .CH = CH - CH + CH. \ (R_a) + HCN$$

$$R_a \longrightarrow CH_2 = CH - C \equiv CH \text{ (rearrangement)}$$

$$P \longrightarrow .CH = CH. + .CH = CH - CH = N. \ (R_b)$$

$$R_b \longrightarrow CH_2 = CH - CN \text{ (rearrangement)}$$

Then R_a or R_b could react with pyridine to form more polymer or other product. A larger surface could help these radicals rearrange or recombine before interaction with the reactant.

Rate equations for non steady-state consecutive-parallel[15] mechanisms were tried but did not fit the data; thus, it was concluded that steady-state had been reached.

Conclusion

From product and kinetic data the following conclusion can be drawn: there is a parallel in the formation of volatile products and in evidence for auto catalysis. At lower temperatures the reaction is first-order and no volatile products are obtained, only polymeric tars. As the temperature increases sufficient energy is available to cause additional ring fragmentation, leading to volatile products, and subsequently these fragments or products interact with pyridine to accelerate its pyrolysis. In order to determine under what conditions NO forms from pyridine oxidation, it will be necessary to determine the rate and products of oxidative pyrolysis (i.e. fuel rich conditions).

APPENDIX A

Kinetic Data

Symbols

c_o = initial concentration of pyridine (mmoles/l)

t = contact time (sec.)

X = concentration of pyridine reacted (mmoles/l)

F = X/c_o = fraction of pyridine decomposed

c = concentration of pyridine at time, t (mmoles/l)

$\%C_o$ = mole per cent of pyridine in carrier gas

r = X/t = rate pyridine decomposition (mmoles/l sec)

HCN = HCN concentration (mmoles/l)

r(HCN) = rate of HCN formation (mmoles/l sec)

A. Medium Reactor

Data at 875°C

No.	$\%C_o$	c_o	t	F	c	X	r	r/c
1	0.50	0.0520	2.00	0.160	0.0437	0.0083	0.0042	0.0961
2	1.00	0.1040	2.00	0.152	0.0882	0.0158	0.0079	0.0896
3	2.00	0.2080	2.00	0.145	0.1778	0.0302	0.0016	0.0899
4	0.25	0.0026	1.00	0.075	0.0239	0.0021	0.0021	0.0879
5	0.50	0.0052	1.00	0.072	0.0477	0.0043	0.0043	0.0901
6	1.00	0.0104	1.00	0.050	0.0946	0.0054	0.0094	0.0937

Data at 900°C

No.	$\%C_o$	c_o	t	F	c	X	r	r/c
7	0.25	0.0254	0.25	0.061	0.0239	0.0016	0.0062	0.260
8	0.50	0.0509	0.25	0.040	0.0489	0.0020	0.0081	0.167
9	0.25	0.0254	0.50	0.092	0.0231	0,0023	0.0047	0.203
10	0.50	0.0509	0.50	0.081	0.0468	0.0041	0.0082	0.175
11	1.00	0.1018	0.50	0.060	0.0954	0.0061	0.0122	0.128
12	2.00	0.2036	0.50	0.070	0.1893	0.0142	0.0285	0.151
13	0.25	0.0254	1.00	0.193	0.0205	0.0049	0.0049	0.239
14	0.50	0.0509	1.00	0.122	0.0447	0.0062	0.0062	0.139
15	1.00	0.1018	1.00	0.089	0.0927	0.0091	0.0091	0.098
16	2.00	0.2036	1.00	0.158	0.1714	0.0322	0.0322	0.188
17	0.50	0.0509	2.00	0.214	0.0400	0.0109	0.0054	0.136
18	1.00	0.1018	2.00	0.295	0.0718	0.0300	0.0150	0.209
19	2.00	0.2036	2.00	0.239	0.1549	0.0457	0.0243	0.157
20	0.50	0.0509	4.00	0.258	0.0378	0.0131	0.0033	0.0087
21	1.00	0.1018	4.00	0.278	0.0735	0.0283	0.0074	0.0096

Data at 925°C

No.	$\%C_o$	c_o	t	F	c	X	r	r/c
22	0.50	0.0498	0.50	0.105	0.0446	0.0052	0.0104	0.234
23	1.00	0.0997	0.50	0.116	0.0881	0.0116	0.0232	0.262
24	2.00	0.1993	0.50	0.130	0.1734	0.0259	0.0518	0.298
25	0.50	0.0498	1.00	0.244	0.0377	0.0122	0.0122	0.322
26	1.00	0.0997	1.00	0.276	0.0722	0.0275	0.0275	0.382
27	2.00	0.1993	1.00	0.284	0.1427	0.0566	0.0566	0.396

Data at 950°C

No.	$\%C_o$	c_o	t	F	c	X	r	r/c	HCN	r(HCN)	r(HCN)/c
28	0.25	0.0244	0.25	0.101	0.0219	0.0025	0.0099	0.449			
29	0.50	0.0488	0.25	0.114	0.0432	0.0056	0.0222	0.515			
30	1.00	0.0976	0.25	0.086	0.0892	0.0084	0.0336	0.376			
31	0.25	0.0244	0.50	0.115	0.0216	0.0028	0.0056	0.260	0.0037	0.0074	.3426
32	0.50	0.0488	0.50	0.183	0.0399	0.0089	0.0179	0.448	0.0046	0.0092	.2306
33	1.00	0.0976	0.50	0.269	0.0714	0.0263	0.0525	0.736	0.0058	0.0116	.1625
34	2.00	0.1953	0.50	0.273	0.1420	0.0533	0.1066	0.751	0.0092	0.0184	.1296
35	0.25	0.0244	1.00	0.233	0.0187	0.0057	0.0057	0.304	0.0070	0.0070	.3743
36	0.50	0.0488	1.00	0.294	0.0345	0.0144	0.0144	0.416	0.0080	0.0080	.2319
37	1.00	0.0976	1.00	0.357	0.0628	0.0349	0.0349	0.555	0.0130	0.0130	.2070
38	2.00	0.1953	1.00	0.392	0.1187	0.0765	0.0765	0.645	0.0188	0.0188	.1584
39	0.25	0.0244	2.00	0.273	0.0177	0.0067	0.0033	0.188			
40	0.50	0.0488	2.00	0.364	0.0310	0.0178	0.0089	0.286	0.0053	0.0077	.2484
41	1.00	0.0976	2.00	0.483	0.0505	0.0472	0.0236	0.467	0.0183	0.0092	.1822
42	2.00	0.1953	2.00	0.581	0.0818	0.1134	0.0567	0.693	0.0249	0.0125	.1528

Data at 975°C

No.	%C_o	c_o	t	F	c	X	r	r/c	HCN	r(HCN)	r(HCN)/c
43	0.25	0.0239	0.25	0.141	0.0205	0.0034	0.0135	0.657	0.0031	0.0124	.6049
44	0.50	0.0478	0.25	0.113	0.0424	0.0054	0.0216	0.509	0.0060	0.0240	.5660
45	1.00	0.0957	0.25	0.142	0.0821	0.0136	0.0543	0.662	0.0104	0.0416	.5067
46	0.50	0.0478	0.50	0.145	0.0409	0.0069	0.0139	0.339	0.0123	0.0246	.6015
47	1.00	0.0957	0.50	0.363	0.0609	0.0347	0.0695	1.139	0.0143	0.0286	.4096
48	2.00	0.1913	0.50	0.407	0.1135	0.0779	0.1558	1.373	0.0245	0.0490	.4317
49	0.25	0.0239	1.00	0.406	0.0142	0.0097	0.0097	0.684	0.0092	0.0092	.6479
50	0.50	0.0478	1.00	0.231	0.0368	0.0110	0.0110	0.300	0.0127	0.0127	.3450
51	1.00	0.0957	1.00	0.322	0.0649	0.0308	0.0308	0.475	0.0188	0.0188	.2897
52	2.00	0.1913	1.00	0.649	0.0672	0.1242	0.1242	1.849	0.0276	0.0276	.4107
53	0.50	0.0478	2.00	0.364	0.0304	0.0174	0.0087	0.286	0.0262	0.0131	.4309
54	1.00	0.0957	2.00	0.483	0.0495	0.0462	0.0231	0.467	0.0358	0.0179	.3616

Data at 1000°C

No.	$\%C_o$	c_o	t	F	c	X	r	r/c	HCN	r(HCN)	r(HNC)/c
55	0.25	0.0234	0.25	0.334	0.0156	0.0078	0.0313	2.006	0.0050	0.0200	1.2821
56	0.50	0.0469	0.25	0.221	0.0365	0.0104	0.0415	1.135	0.0169	0.0676	1.8521
57	1.00	0.0938	0.25	0.202	0.0748	0.0189	0.0758	1.012	0.0258	0.1032	1.3797
58	0.25	0.0234	0.50	0.454	0.0128	0.0106	0.0213	1.663	0.0157	0.0314	2.4531
59	0.50	0.0469	0.50	0.535	0.0218	0.0251	0.0502	2.301	0.0236	0.0472	2.1651
60	1.00	0.0938	0.50	0.686	0.0295	0.0643	0.1287	4.369	0.0384	0.0768	2.6034
61	2.00	0.1876	0.50	0.807	0.0362	0.1514	0.3028	8.363	0.0570	0.1140	3.1492
62	0.25	0.0234	1.00	0.588	0.0097	0.0138	0.0138	1.427	0.0190	0.0190	1.9588
63	0.50	0.0469	1.00	0.634	0.0172	0.0297	0.0297	1.732	0.0329	0.0329	1.9130
64	1.00	0.0938	1.00	0.772	0.0214	0.0724	0.0724	3.386	0.0460	0.0460	2.1495
65	2.00	0.1876	1.00	0.831	0.0317	0.1559	0.1559	4.917	0.0651	0.0651	2.0536
66	0.25	0.0234	2.00	0.739	0.0061	0.0173	0.0087	1.416			
67	0.50	0.0469	2.00	0.762	0.0112	0.0357	0.0179	1.601			
68[a]	1.00	0.0938	2.00	0.916	0.0079	0.0859	0.0430	5.452			
69[b]	2.00	0.1876	2.00	0.931	0.0129	0.1746	0.0873	6.746	0.0747	0.0374	2.8992

a,b. These data points are from high extent of reaction. They were not included in the determination of the rate constants at 1000°C.

$(CN)_2$ Acceleration Effect Data

No.	Temperature, °C	t	$\%C_o$	Helium carrier F	2% $(CN)_2$ in helium F
70	975	1.00	1.00	0.322	0.604
71	975	1.00	0.50	0.236	0.620
72	900	1.00	1.00	0.095	0.285
73	925	1.00	1.00	0.234	0.438

B. Small Reactor

Data at 975°C

No.	$\%C_o$	c_o	t	F	c	X	r	r/c
74	0.50	0.0478	0.50	0.050	0.0454	0.0024	0.0048	0.105
75	1.00	0.0957	0.50	0.212	0.0754	0.0203	0.0406	0.538
76	2.00	0.1913	0.50	0.241	0.1452	0.0461	0.0922	0.635
77	0.50	0.0478	1.00	0.101	0.0430	0.0048	0.0048	0.112
78	1.00	0.0957	1.00	0.220	0.0746	0.0210	0.0211	0.282
79	2.00	0.1913	1.00	0.333	0.1276	0.0637	0.0637	0.499

Data at 1000°C

No.	$\%C_o$	c_o	t	F	c	X	r	r/c
80	0.50	0.0469	0.50	0.204	0.0373	0.0096	0.0191	0.513
81	1.00	0.0938	0.50	0.266	0.0688	0.0249	0.0499	0.725
82	2.00	0.1876	0.50	0.408	0.1110	0.0765	0.1531	1.378
83	0.50	0.0469	1.00	0.337	0.0311	0.0158	0.0158	0.508
84	1.00	0.0938	1.00	0.502	0.0467	0.0471	0.0471	1.008
85	2.00	0.1876	1.00	0.552	0.0840	0.1035	0.1035	1.232

C. Large Reactor

Data at 975°C

No.	$\%C_o$	c_o	t	F	c	X	r	r/c	HCN	r(HCN)/c
86	0.50	0.0478	0.50	0.253	.0357	.0120	.0242	0.678	.0062	.3473
87	1.00	0.0957	0.50	0.319	.0652	.0305	.0611	0.937	.0162	.4969
88	0.50	0.0478	1.00	0.228	.0369	.0109	.0109	0.295	.0189	.5122
89	1.00	0.0957	1.00	0.563	.0418	.0539	.0539	1.289	.0288	.6889
90	2.00	0.1913	1.00	0.813	.0358	.1555	.1555	4.344	.0293	.8184

APPENDIX B

Calibration Data

Helium Flow Rate

A. Small Capillary - (0.5 mm x 6 cm)

Pressure Drop, cm	Flow rate, ml/sec. at STP
4.4	3.1
7.7	5.4
11.6	8.0
15.6	10.7
19.1	12.9
22.6	15.1

thus, flow rate = $(0.689)(\Delta p)$ ml/sec at 0^{o}C and 760 mm Hg. total pressure. Data was obtained at 28.6^{o}C and 745 mm Hg. total pressure.

B. Large Capillary - (1.0 mm x 6 cm)

Pressure drop, cm	Flow rate, ml/sec at STP
7.9	20.2
12.0	29.3
15.8	37.5
22.3	49.4

thus, flow rate = $(2.40)(\Delta p)$ ml/sec at 0^{o}C and 760 mm Hg. total pressure. Data was obtained at 28.3^{o}C and 745 mm Hg. total pressure.

Rate of Injection

A. 1 cc Syringe - (large drive gear)

Syringe drive potentiometer setting	Rate of injection, µl of sec
500	0.810
400	0.650
200	0.328
100	0.162
40	0.072

thus, syringe drive potentiometer setting (620) (µl/sec of pyridine)
The molar and weight flow rates were calculated using 79.10 gms/mole and 0.978 gm/ml[8] as the molecular weight and density of pyridine respectively. The temperature at the syringe during any given run was 25 $\pm$ 2°C; this relative consistency resulted from the close proximity of the syringe to the furance, thus, reducing the magnitude of normal room temperature fluctuations.

B. 1 cc Syringe - (small drive gear)

Syringe drive potentiometer setting	Rate of injection, µl of sec
200	0.127
400	0.248
800	0.497

thus, potentiometer dial setting = (1.60×10^3)(µl/sec of pyridine)

Gas Chromatographic HCN Analysis Data

100 x Peak height ratio HCN/1% pyridine	HCN concentration mmoles/l x 10^2 determined by titration
22.4	2.50
18.4	2.11
10.1	1.11
36.1	4.42

Thus, HCN concentration = (0.117) (peak height ratio)

APPENDIX C

Analysis of Uncertainties

Uncertainties for individual measurements and their influence on the final results were estimated in the following manner:

1. The uncertainty in the helium flow rate depended upon the magnitude of the pressure drop which could be read to $\pm$ 0.1 cm. The lowest and highest readings for the medium reactor were 5.0 cm and 20.0 cm respectively. Thus, the maximum and minimum uncertainties were 0.1/5.0 = 2.0% and 0.1/20.0 = 0.5%. Maximum uncertainty, therefore, occurred at long contact times.
2. Uncertainty in the amount of pyridine injected was based on the injection rate. The limit of reproducibility determined the uncertainty in injection rate which was felt to be about $\pm$ 0.001 microliters/sec. Thus, the largest uncertainty occurred at the lowest concentration (.25%) and the longest contact time (2 sec) where the rate was 0.04 microliters/sec and was 2.5%. The smallest uncertainty was about .04% when the injection rate was 2.6 microliters/sec. Uncertainties in time measurements were considered negligible.

3. The volume of the reactor was measured to about $\pm$ 1 ml and the total volume was approximately 39 ml. Hence, the uncertainty was 1/39 = 2.5%. This source of uncertainty was not random and consequently did not contribute to the random behavior of the individual values, rather, was added to the final uncertainty in the rate constants. Due to the very low coefficient of thermal expansion of Vycor, volume changes accompanying temperature changes were considered negligible.
4. The uncertainty in the gas chromatographic determination of the amount of unreacted pyridine arose principally from random instrumental factors which resulted in irreproducibility. Typically, these uncertainties were 1/30 = 3.3%.
5. Uncertainties in initial concentration arose from (1) and (2) while those in final concentration were related to (1), (2), and (4).

   Uncertainty in initial concentration--

   Maximum: 2.0% + 2.5% = 4.5%

   Minimum: 0.5% + .04% = .54%

   Uncertainty in final concentration--

   Maximum: 2.0% + 2.5% + 3.3% = 7.8%

   Minimum: 0.5% + 0.04% + 3.3% = 3.8%
6. Uncertainties in contact time resulted principally from those in the helium flow rate, i.e., 0.5% to 2.0%.

However, minor contributions result from uncertainties in the injection rate and changes in gas volume accompanying pyrolysis. This latter point was further complicated by the formation of non-volatile residues from the decomposition products. It was estimated that at short contact times and high concentrations, the uncertainty in the gas volume had its minimum value of 0.1% and 0.7% as its maximum value at long contact times and low concentrations. This source of uncertainty resulted from uncertainty in extent of reaction and from the fact that the formation of polymeric residue reduced the volume of gases.

Uncertainty in contact time---

Maximum: 2.0% + 0.7% = 2.7%

Minimum: 0.5% + 0.1% = 0.6%

Uncertainties in the reactor's volume contributes to the uncertainty in contact time; however, this has been discussed in (3).

7. Uncertainties in the rate constants depend on the total uncertainty in the difference between initial and final concentrations which is highly dependent on the extent of reaction. The following examples are illustrative:

(a) If the initial concentration (run. No. 28)

c_o = 0.0244 mmoles/lit and the final concentration

c = 0.0219 mmoles/lit

t = 0.25 sec

T = 950°C

Since the contact time is low (high flow rate), the minimum concentration uncertainty is applicable.

$X = c_o - c = 0.0244 \pm 0.0244 \times 0.5\% - 0.0219 \pm 0.0219 \times 3.84\% =$

$0.0244 \pm 0.0001 - 0.0219 \pm 0.0008 = 0.0025 \pm 0.0009$

Therefore, the total uncertainty in X is $\pm$ 0.0009/.0025

$\pm$ 36%

(b) If the initial concentration (run no. 42)

c_o = 0.1953 mmoles/lit and the final concentration

c = 0.0818 mmoles/lit

t = 2.00 sec

T = 950°C

Since the contact time is long, but the concentration high, an uncertainty value greater than minimum but less than maximum is applicable.

$X = c_o - c = 0.1953 \pm 0.1953 \times 3\% - 0.0818 \pm 0.0818 \times 5.5\%$

$= 0.1953 \pm .0059 - 0.0818 \pm .0045$

Therefore, the total uncertainty of X is 0.1135 $\pm$ 9.2%

The uncertainty in a calculated rate (X/t) value for a low contact time and low extent of reaction is 36 $\pm$ .7 = 36.7%. For a high contact

time and high extent of reaction, the uncertainty in the rate is 9 + 2.7 = 11.7%. Thus, there is a leveling effect since high flow rates, which correspond to low uncertainties in concentration, produce low extents of reaction, which yield high uncertainties due to small values of X and vice versa. The lower uncertainty in Example (b) is not only because of high concentration but also due to the high extent of reaction as compared to Example (a).

Thus, rate values, calculated from low temperature experiments would have a probable maximum uncertainty of about 40% (used in Table below), where those resulting from high temperature experiments would have a lower maximum uncertainty of about 10% due to the high extent of the reaction.

8. The above calculations describe the maximum deviation from the mean that a data point can have under a particular set of conditions and are tabulated below as predicted uncertainty. Rate constants were calculated from least square intercepts and slopes respectively of plots of r/c versus X where $R = k_1c + k_2cX$. Values are tabulated below:

Temp. oC	Mean Values k_1	k_2	Predicted (max.) uncertainty		Observed deviation (95% confid. level)	
875	0.090	-	0.037	-	0.004	-
900	.158	-	0.068	-	0.030	-
925	0.249	2.87	0.099	1.14	0.040	1.38
950	0.367	3.74	0.147	1.50	0.066	1.58
975	0.404	11.47	0.162	4.59	0.156	3.02
1000	0.986	36.71	0.394	14.70	0.500	6.18

It can be seen that the observed deviations (95% confidence level) fall within the range predicted from the treatment of uncertainties.

APPENDIX D

Sample Calculation of the Rate of Production of HCN

NOTATIONS

H_{HCN} Peak heights of HCN (mm)

$H_{pyridine}$ Peak height of Pyridine (mm) through by pass

V_{AgNO_3} Volume of N/40 $AgNO_3$ used for titration (cc)

t Length of time HCN trapped in NaOH (sec)

t_c Contact time (sec)

V Reactor volume (cc)

u Flow rate through reactor (cc/sec)

Given:

H_{HCN}	=	16
$H_{pyridine}$	=	137
Mole % Pyridine	=	2
V_{AgNO_3}	=	34.2
t	=	1720
t_c	=	1 sec
V	=	39.25 cc
1ml $AgNO_3$	=	5×10^{-5} mole HCN

Find:

1) Total number of moles of HCN produced

2) Number of moles of HCN/sec

3) HCN concentration in the gas mixture, mmoles/cc, C.

4) Rate of formation of HCN

5). Show relation of standardized peak height and HCN concentration

Solutions:

1. 1ml $AgNO_3$ = 5×10^{-5} mole HCN

   Hence, 34.2 ml = 1.71×10^{-3} mole

2. HCN/sec. = $\frac{1.71 \times 10^{-3}}{1720}$ = 9.94×10^{-7} mole/sec

3. $u = \frac{V}{t_c} = \frac{39.24}{1} = 39.24$ cc/sec

   HCN mmole/cc = $\frac{9.94 \times 10^{-7} \text{ mole/sec}}{39.24 \text{ cc/sec}}$

   = 2.5×10^{-5} mmole/cc

4. Rate of formation of HCN = $\frac{C - C_o}{t_c}$

   = $\frac{2.5 \times 10^{-5}}{1}$

   = 2.5×10^{-5} mmole/cc sec

5. Standardized peak height

   = $\frac{\text{peak height of HCN}}{\text{peak height of 1\% Pyridine}} \times 100$

   = $\frac{16}{137/2} \times 100 = 23.4$

   23.4 is proporational to 2.5×10^{-5} mmole/cc of HCN

BIBLIOGRAPHY

1. R. Snyder, Anal. Chem., 41, 314 (1969).

2. C.F. Roth, Ber., 19, 360, 1886.

3. C.D. Hurd, and J.I. Simon, J. Am. Chem. Soc., 84, 4519, (1962).

4. A.E. Axworthy and M. Schuman, "Investigation of the Mechanism and Chemistry of Fuel Nitrogen Conversion to Nitrogen Oxides in Combustion", Coal Combustion Symposium, E.P.A., Traingle Park, N.C., June 1973.

5. A.A. Frost and R.G. Pearson, "Kinetics and Mechanism", John Wiley and Sons, Inc., New York, 1963, p. 183.

6. O.A. Hougen and K.M. Watson, "Chemical Process Principles - III, Kinetics and Catalysis", John Wiley and Sons, Inc., New York, 1955.

7. J.M. Sullivan and T.J. Houser, Chem. and Ind., 1057, 1965.

8. "Handbook of Chemistry and Physics", 45th ed., The Chemical Rubber Company, 1964-5, E-49.

9. W. Scott and N.H. Furman, "Standard Methods of Chemical Analysis", D. Van Nostrand Co., New York, vol. 1, 1962, p. 39.

10. "Index of Mass Spectral Data", American Chemical Society for Testing and Materials", (1969).

11. T.W. Asmus and T.J. Houser, J. Phys. Chem., 73, 2555, (1969).

12. J.H. Beynon and A.E. Williams, "Mass and Abundance Tables for Use in Mass Spectrometry", Elsevier Publishing Co., N.Y., 1963.

13. K.J. Laidler, "Chemical Kinetics, McGraw-Hill Book Company, New York, 1965, p. 36.

14. J.S. Dewar, A.J. Harget, N. Trinajstic, J. Am. Chem. Soc., 91, 6321, (1969).

15. T.J. Houser, J. Chem. Phys., 50, 3962, (1969).